Title

Mechanical and Thermal Analysis of an HTS Superconducting Magnet for an Achromatic Gantry for Proton Therapy

Journal

IEEE Transactions on Applied Superconductivity, 32(6)

ISSN

1051-8223

Authors

Fernandez, Jose Luis Rudeiros

Brouwer, Lucas

Mallon, Philip

et al.

Publication Date

2022

DOI

10.1109/tasc.2022.3158366

Peer reviewed

Mechanical and thermal analysis of an HTS superconducting magnet for an achromatic gantry for proton therapy

J. L. Rudeiros Fernández, L. Brouwer, P. Mallon, S. Prestemon, J. Qiang, T. Shen, R. Teyber

ABSTRACT **—The mechanical and thermal analysis of the super-conducting magnets, forming an innovative fixed-field bending section for use in a proton therapy gantry, are here presented. The design concept has a large momentum acceptance, covering the full proton energy range of 70 to 220 MeV with fixed-field in the superconducting magnets, and uses a simple magnet geometry based on double-pancake high temperature superconductor coils. The main planned steps for the assembly and fabrication of the magnets are discussed. The mechanical and thermal analyses of the magnet are also discussed.**

I. Introduction

The treatment of cancer tumors with ion-beam therapy uses the local deposition of energy at the Bragg peak of the ions. An example of this type of installation is the Gantry 2, located in the Paul Scherrer Institute [1]. The main challenges of this type of facility are the scale and cost of the infrastructure, where the weight and size of the gantry are some of the important parameters driving the final cost.

The innovative concept of using a combination of two identical superconducting bend magnets working at a fixed field in a proton therapy gantry, allows for a light and compact design, while being able to deliver protons over a range of 70 to 220 MeV, and is a further simplification of the design presented in [2]. The proposed concept uses the high-temperature superconductor (HTS) Bi-2223, as it has been shown to be competitive in terms of reduced manufacturing cost and improved thermal stability [3], [4]. The new design, as an HTS technology demonstrator, further simplifies the coil design, reducing the field and increasing the weight as a trade-off. The overall design also reduces the number of quadrupoles from six [2], to four.

The gantry, schematically represented in Fig. 1, is conceived as achromatic, allowing the dipole superconducting magnets to operate at a constant field, and therefore avoiding the technical challenges and risks of fast-field ramping required in other designs to accommodate various beam energies, and may avoid magnet training before use. The proposed design of the superconducting magnets consists of a series of straight, double-pancake coils embedded in an iron yoke. The coils are made of Bi-2223/Ag (DI-BSCCO) HTi-CA tape, and produce a maximum magnetic field of about 2.5 T at 12 K, with a multi-stage conduction cooling system.

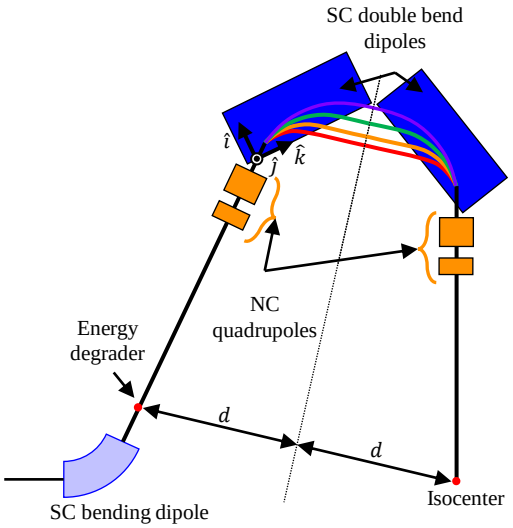

Fig. 1. The proposed concept for the fixed field proton gantry, based on the concept in [2].

This paper presents the mechanical and thermal analysis of the magnet, based on finite element simulations. The main components of the mechanical structure, winding of the coils, assembly, and values of stress in the conductor due to the electromagnetic forces are discussed. Furthermore, the expected temperature gradients within the superconducting coils are also addressed.

II. Superconducting magnet design

A. Magnet components and configuration

The gantry-magnet system is designed for proton therapy, making use of an achromatic concept and therefore allowing for the magnets to operate at a fixed field. As a consequence, the ramping of the superconducting magnets is eliminated, also allowing for a relatively simple and cost-effective design using HTS. At the same time, the iron design allows for a minimization of the fringe field. The details of the conductor chosen for the magnet are included in Table I.

The cross section and constituents of the superconducting magnet are summarized in Fig. 2. The main parameters of the

Manuscript created November, 2021. This work was supported by the U.S. Department of Energy, Office of Science, Office of High Energy Physics, through the HEP Stewardship program, and in partnership with the Paul Scherrer Institut and Varian.

J. L. Rudeiros Fernández, L. Brouwer, P. Mallon, S. Prestemon, J. Qiang, T. Shen, R. Teyber are with the Lawrence Berkeley National Laboratory, Berkeley, CA 94820 USA. (email: jrudeirosfernandez@lbl.gov)

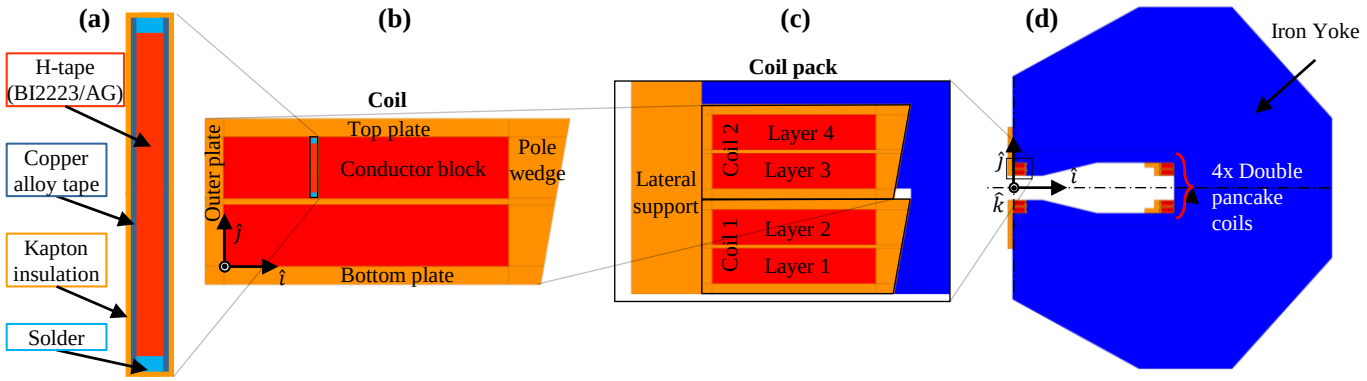

Fig. 2. Main elements of the magnet forming the achromatic twin magnet system. (a) Schematic representation of the main components of the Bi-2223/Ag (DI-BSCCO) tape, based on [5], [6]. (b) Coil cross section. Each layer is separated by an inter-layer. The double pancake is encapsulated by a series of copper plates, to be all impregnated with resin in a single block forming the coil. (c) The coil pack is formed by a pair of coils which are held in position by lateral supports within the yoke structure. (d) The full cross section of the superconducting magnet.

TABLE I
CONDUCTOR PARAMETERS

Bi-2223 (DI-BSCCO) Tape, HTi-CA

Property	Value
Height (mm), insulated	4.6 ± 0.1
Thickness (mm), insulated	0.4 ± 0.02
I_c (A) at 77 K , self field	$\geq$ 170
Insulation polyimide tape thickness (μm)	12.5[a]

[a] The insulation tape is wrapped around the conductor with a 50 % overlap.

magnet are listed in Table II. The magnet along the auxiliary systems will form a cryocooled superconducting magnet, to be operated at 12 K.

TABLE II
SUPERCONDUCTING MAGNET PARAMETERS

Property	Value
Magnet's full aperture (mm)	50
Peak B_y field (T) on the magnet's midplane	2.46
Peak $\|B\|$ field (T) in the conductor	2.42
Operating temperature (K)	12
Operating current (A), I_{op}	340
Load line margin (%)	30[a]
Number of double pancake coils	4
Number of layers per coil	2
Turns per layer	58
Conductor length per coil (m)	482.6
Coil inner diameter (mm)	281
Coil physical length (mm)	1926
Coil weight (kg), approx.	8.5
Yoke length (mm)	1780
Magnet weight (kg), approx.	5300

[a] Load line margin computed based on the perpendicular field to the tape, i.e. $|B_x|$.

The main fabrication steps are:

1) Coil winding: the coil is wound in the shape of a double pancake with support provided by the pole piece and bottom plate.
2) Resin impregnation of the coils: After winding, the outer and top plates are placed in position. The assembly is confined in a closed mold ready for impregnation.
3) Assembly of the coils within the iron yoke: The coils are placed inside the laminated yoke structure. Lateral supports are attached to the yoke to ensure the nominal position of the coils.

B. Magnetic considerations

The magnitude and direction of **B** in the conductor blocks are shown in Fig. 3. The resulting Lorentz forces are summarized for each layer and side (i.e., left and right) in Table III. The main magnetic curves are illustrated in Fig. 4. The critical values of the peak field within the conductor for the left and right sides of the magnet, according to the positions referenced in Fig. 2 (d), are shown in Fig. 4 (b).

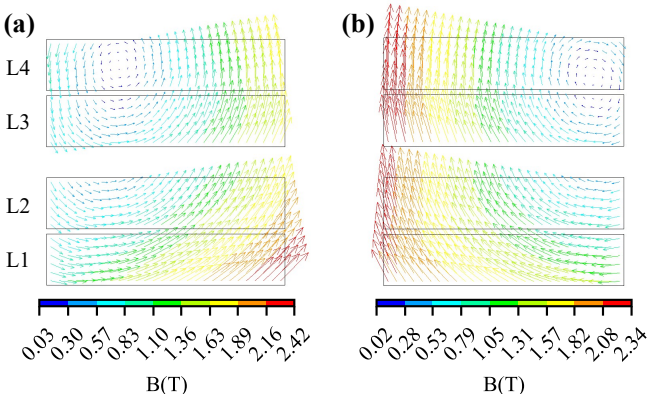

Fig. 3. **B** field. Left-Right orientation based on Fig. 2 (c). (a) Left side of the magnet. (b) Right side of the magnet.

C. Mechanical analysis

A finite element model was developed in ANSYS to investigate the stress state of the conductor and coil structure during the powering of the magnet due to the Lorentz forces. The main model geometry, boundary conditions, and results are summarized in Fig. 5. The maximum von misses stress in the model is found in the iron yoke with a value of 57 MPa. The

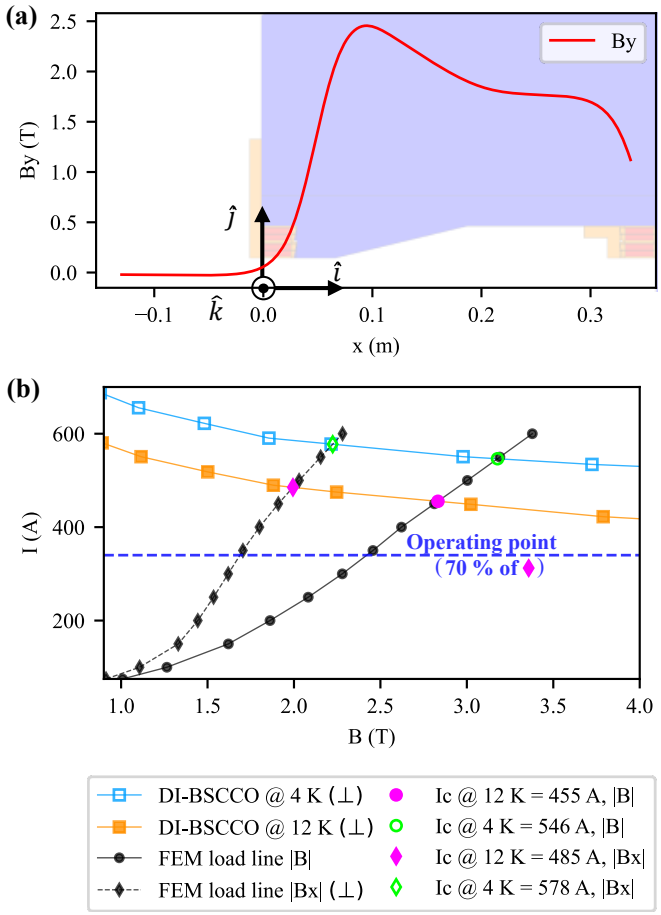

Fig. 4. Magnetic design. (a) B_y field in the x-direction. The magnetic field profile is the result of an optimization process, where the magnets should provide the required vertical field by the optics in all regions sampled by the beam. The vertical field is created by 4 double pancake coils, where the field is shaped with the help of the iron geometry. (b) Load line of the magnet. Critical current fittings of (DI-BSCCO) tape from [6].

TABLE III
SUMMARY OF LORENTZ FORCES

Coil	Layer	Position	Force (kN) x	Force (kN) y
1	1	Left	-14	24
1	2	Left	-12	13
2	3	Left	-10	8
2	4	Left	-10	-1
1	1	Right	18	21
1	2	Right	19	11
2	3	Right	20	7
2	4	Right	19	-2

maximum equivalent von misses stress in the conductor is in the top corner of layer 3 with a value of 11 MPa. Furthermore, the maximum values of normal and shear stress along the interfaces between the conductor and the additional plates included in the impregnation are low. The debonding stresses, i.e., tension in the normal direction and shear stress, remained below 2 MPa.

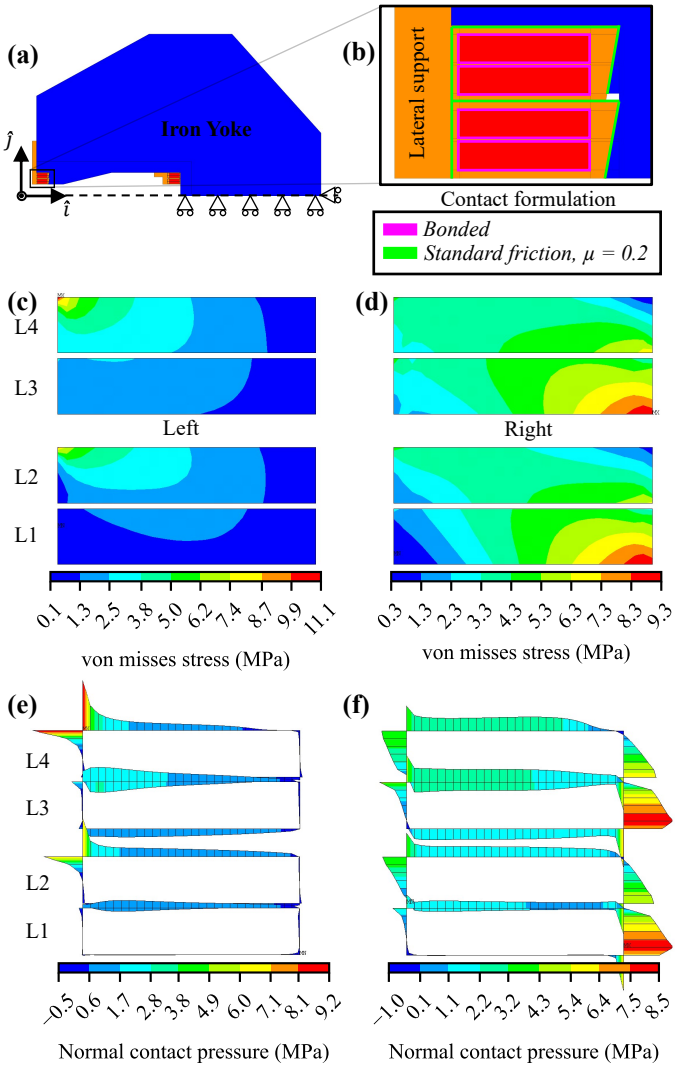

Fig. 5. Mechanical finite element model and results. (a) The coils are placed inside the laminated yoke structure and held in place by the action of the respective lateral support. (b) Contact formulation for the coil packs. Due to the Lorentz forces, the coils are pushed outwards and up. In this design, the coils are allowed to slide on the support surfaces and on each other. (c) Left side, equivalent von misses stress for the conductor. (d) Right side, equivalent von misses stress for the conductor. (e) Left side, normal contact pressure in the boundaries of the conductor block. (f) Right side, normal contact pressure in the boundaries of the conductor block.

D. Prototyping

In a first step to develop the manufacturing procedures required for this magnet, and to investigate the sensitivity of the conductor to bending strain, an experiment was carried out in which the DI-BSCCO tape was hard-bent into two different profiles into a G-10 plate, with a radius of 1500 and 2000 mm, as illustrated in Fig. 6 (a). The hard-bends were chosen to replicate the required layer-jump required in the double pancake winding configuration. The two specimens were then clamped with an additional G-10 plate and immersed in liquid nitrogen, where the critical current (I_c) of each tape was measured, Fig. 6 (b). The measurements revealed a value of I_c about 193 A at 77 K, with a ramp rate of 2 A m^{-1}. The next step contemplates 10 turns winding test as illustrated in Fig. 6 (d).

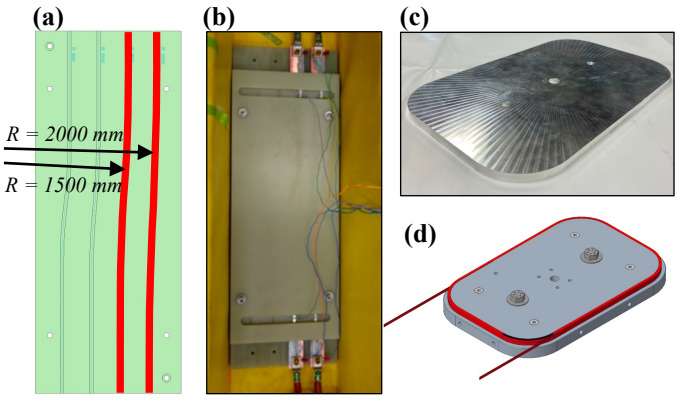

Fig. 6. Prototyping. (a) G-10 plate used as a sample-holder for the hard-bent tape. One specimen was bent into layer jump with a 1500 mm radius and a second specimen into a 2000 mm radius. (b) Tapes connected to the power supply within the liquid nitrogen container. (c) Pole piece for the winding test. (d) CAD image representing the planned 10 turn windability test.

E. Thermal analysis

The constructed thermal models might use the individual properties of each material, but when looking at relatively complex models with a large number of winding turns, it becomes more practical to use effective thermal properties. In relation to the thermal conductivity, $\kappa(T)$, based on [7], the fitting equations were of the type:

$$\kappa(T) = 10^{\left(a_0 + a_1 \log_{10} T + a_2 (\log_{10} T)^2 + \ldots + a_n (\log_{10} T)^n\right)} \quad (1)$$

where T is the temperature. The effective thermal conductivity [8], $\kappa_e(T)$ can be estimated from the fitted continuous functions based on (3), considering the components' parallel and perpendicular directions, as shown in Fig. 7 (a).

The local heat dissipated can be estimated based on the voltage appearing in the conductor when operating at conditions close to I_c

$$E = E_0 \left(\frac{I_{op}}{I_c}\right)^n \quad (2)$$

where E_0 is considered as $1 \times 10^{-4}\,\mathrm{V\,m^{-1}}$. The expression can be rewritten to express the heat deposition in terms of volume,

$$\frac{P}{V_{cond}} = \frac{E_0 I_{op}}{A_{cond}} \left(\frac{I_{op}}{I_c}\right)^n \quad (3)$$

where V_{cond} is the volume of the conductor, and A_{cond} is the cross-sectional area of the conductor. If one considers the critical region of the coil in terms of critical current, the volumetric heat deposition in the H-tape is estimated as $243\,\mathrm{W\,m^{-3}}$, or $120\,\mathrm{W\,m^{-3}}$ if the coil is considered as a smeared region.

The 2D and 3D finite element models developed in ANSYS and their respective results are summarized in Fig. 8. A worst-case scenario is explored in both 2D and 3D models where only one out of the four copper plates remains available for heat extraction, which is kept at its extremity at operational temperature, i.e. 12 K. The results of both models indicated that the temperature increase should remain below 0.5 K.

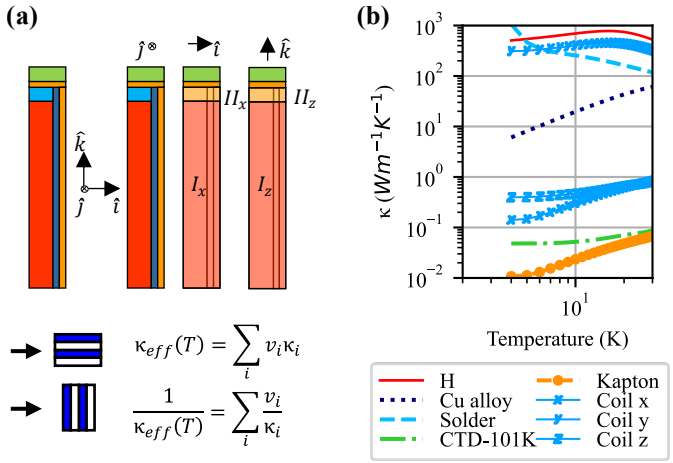

Fig. 7. Thermal conductivity of the materials of the coil model. (a) The effective thermal conductivity of the unit cell of the coil, represented here as a quarter of a tape, can be computed by progressively subdividing the coil in a series of parallel or perpendicular segments. (b) Thermal conductivity properties of the components of the Bi-2223 (DI-BSCCO) HTi-CA tape [9], kapton [7] and a reference resin [10]

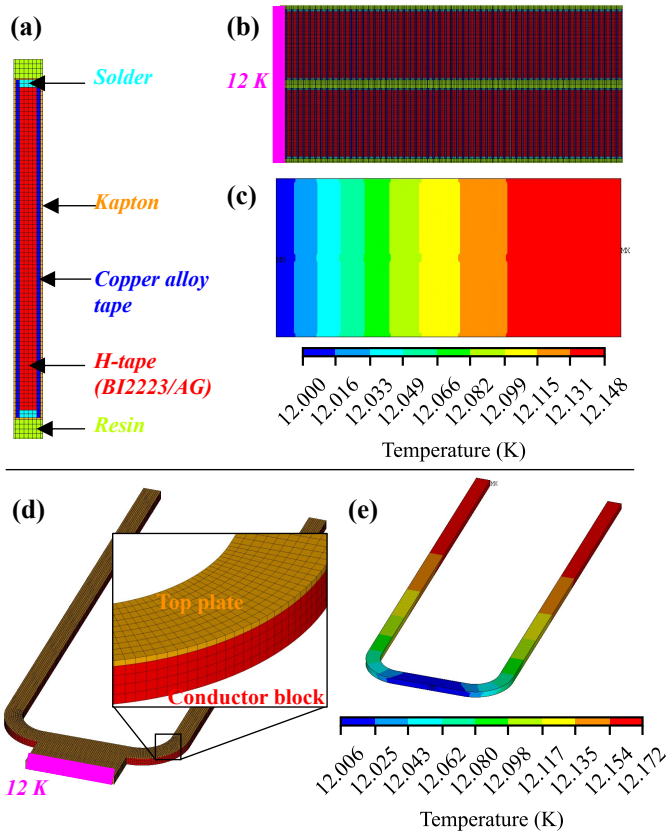

Fig. 8. Thermal analysis summary. (a) Finite element model mesh of the unit cell, i.e. tape, use to reproduce 2D thermal behavior. (b) Assembled 2D cross section of the coil with 58 turns per layer. The operating temperature is imposed in one of the vertical edges of the coil block, while applying the worst case heat deposition of $243\,\mathrm{W\,m^{-3}}$ in the H-tape elements. (c) 2D temperature results. (d) 3D thermal model formed by smeared elements forming the conductor block and a copper top plate. (e) 3D temperature results.

III. Conclusion

The mechanical analysis of the superconducting magnet has shown that the stress levels in the conductor and the magnet structure are acceptable. Furthermore, it has been shown how the strain created in the tape during the hard way bending, required for the layer jump of the double pancake coils, in the measured cases of 1500 and 2000 mm radius, allows for the I_c to remain above specification. Regarding the thermal design of the coil, it has been shown how the copper-based structure around the coil results in adequately low thermal gradients. In conclusion, it has been demonstrated that the mechanical and thermal designs are suitable for the magnet to operate at its nominal conditions.

IV. Acknowledgments

The authors would like to thank Stephane Sanfilippo, Daniela Kiselev, David Meer, Jacobus Maarten Schippers, and Christian Baumgarten of the Paul Scherrer Institute for their collaboration and valuable feedback on gantry design and beam optics.

References

[1] E. Pedroni, R. Bearpark, T. Böhringer, A. Coray, J. Duppich, S. Forss, D. George, M. Grossmann, G. Goitein, C. Hilbes, M. Jermann, S. Lin, A. Lomax, M. Negrazus, M. Schippers, and G. Kotrle, "The PSI Gantry 2: A second generation proton scanning gantry," *Zeitschrift fur Medizinische Physik*, vol. 14, no. 1, pp. 25–34, 2004. [Online]. Available: http://dx.doi.org/10.1078/0939-3889-00194

[2] L. Brouwer, A. Huggins, and W. Wan, "An achromatic gantry for proton therapy with fixed-field superconducting magnets," *International Journal of Modern Physics A*, vol. 34, no. 36, 2019.

[3] R. Teyber, L. Brouwer, A. Godeke, and S. Prestemon, "Thermoeconomic cost optimization of superconducting magnets for proton therapy gantries," *Superconductor Science and Technology*, vol. 33, no. 10, 2020.

[4] A. Godeke, L. Alberty, E. Akcöltekin, R. Babouche, C. Detourbe, R. Nast, C. Radermacher, H. Röcken, A. Roth, M. Schillo, P. V. vom Stein, M. Walpole, J. Wittschen, K. Hayashi, E. Shizuya, H. J. Krooshoop, R. Lubkemann, A. Nijhuis, C. H. Vermeer, W. A. Wessel, J. Krause, J. Wiezoreck, A. Otto, and L. Saraco, "Research at Varian on applied superconductivity for proton therapy," *Superconductor Science and Technology*, vol. 33, no. 6, 2020.

[5] K. Yamazaki, T. Kagiyama, M. Kikuchi, S. Yamade, T. Nakashima, S. Kobayashi, G. Osabe, J. Fujikami, K. Hayashi, and K. Sato, "Recent progress on improvement to mechanical properties of DI-BSCCO wire," *Superconductor Science and Technology*, vol. 25, no. 5, 2012.

[6] K. Sato, *Research, Fabrication and Applications of Bi-2223 HTS Wires*, 2016.

[7] NIST, "Cryogenic material properties," 2021. [Online]. Available: https://trc.nist.gov/cryogenics/materials/materialproperties.htm

[8] J. Wang, J. K. Carson, M. F. North, and D. J. Cleland, "A new approach to modelling the effective thermal conductivity of heterogeneous materials," *International Journal of Heat and Mass Transfer*, vol. 49, no. 17-18, pp. 3075–3083, 2006.

[9] T. Naito, H. Fujishiro, and Y. Yamada, "Thermal Conductivity and Dilatation of Bi-2223/Ag (DI-BSCCO) Superconducting Wire Laminated With Various Thin Alloy Tapes," *IEEE Transactions on Applied Superconductivity*, vol. 28, no. 4, pp. 24–27, 2018.

[10] T. Koettig, W. Maciocha, S. Izquierdo Bermudez, J. Rysti, S. Tavares, F. Cacherat, and J. Bremer, "Thermal conductivity measurements of impregnated Nb3Sn coil samples in the temperature range of 3.5 K to 100 K," *IOP Conference series: Materials science and Engineering*, no. 171, 2017.